

Electrochemical Behavior of Austenitic Stainless Steels Exposed to Acetic Acid Solution

K. Zuñiga-Diaz^{1,3}, C.D. Arrieta-Gonzalez², J. Porcayo-Calderon^{3,*}, J.G. Gonzalez-Rodriguez³, M. Casales-Diaz¹, L. Martinez-Gomez^{1,4}

¹ Instituto de Ciencias Físicas, Universidad Nacional Autónoma de México, Avenida Universidad s/n, 62210 Cuernavaca, MOR, México.

² Tecnológico Nacional de México - Instituto Tecnológico de Zacatepec, Calzada Instituto Tecnológico 27, 62780 Zacatepec, MOR, México

³ CIICAp, Universidad Autónoma del Estado de Morelos, Avenida Universidad 1001, 62209 Cuernavaca, MOR, México.

⁴ Corrosion y Protección (CyP), Buffon 46, 11590 México City, México.

*E-mail: jporcayoc@gmail.com

Received: 17 September 2019 / Accepted: 30 October 2019 / Published: 31 December 2019

In this work, an electrochemical evaluation was carried out for different austenitic stainless steels in an acetic acid solution based on Italian Decree text. The electrochemical performance of the steels was determined by electrochemical techniques such as potentiodynamic polarization curves, measurements of the open circuit potential, linear polarization resistance, and electrochemical impedance spectroscopy. Although the steels show a high corrosion resistance, the specific performance of each one depends on both the chemical composition and the microstructural characteristics. It was found that an increase in the Cr content decreases the corrosion resistance, but precipitates and inclusions decrease it considerably, thus favoring the release of metallic ions into the electrolyte. In addition, the capacitive properties of the protective oxide depend on both the degree of Cr enrichment degree and its thickness.

Keywords: Corrosion, austenitic stainless steel, food contact, electrochemical techniques, acetic acid.

1. INTRODUCTION

Stainless steels are widely used for transportation, processing, and the storage of both food and beverages due to their excellent corrosion resistance and good mechanical properties. The most commonly used ones are the austenitic stainless steels, which are characterized by a minimum of 16% Cr and 6% Ni (wt. %). The corrosion resistance is due to the ability to develop a thin self-healing passive film based on Cr. Stainless steels 304 and 316 are used most often [1-6].

However, other alloy elements can also be incorporated into the passive film structure, so its protective capacity depends on both the degree of Cr enrichment and the presence of other alloy elements, such as Fe, Ni, Mn, Mo, S, Ti, and Nb. In addition, depending on the pH of the solution, these metallic elements can leach out, which affects the stability of the protective film and can contaminate food. The release of metallic ions can occur by electrochemical, chemical, and physical processes. Examples of these processes are corrosion, dissolution, and friction, respectively [4, 7]. Food contamination by both metal ions released or metal complexes that form can alter the organoleptic characteristics of food and pose a risk to consumers. Some of these released metal elements can be beneficial in trace amounts, but depending on their chemical form and concentration, they can lead to adverse health effects [3, 6, 8]. Therefore, it is of great interest to determine the performance of all metallic materials that will be in contact with food [9].

Many studies have reported on the performance of materials when they are in contact with food fluids, which were based on test guides to ensure safety, such as the Council of Europe (CoE) guidelines [10] and the Italian Decree [11]. The main difference between the procedures is the type of electrolyte used to simulate acidic food conditions. The CoE recommends the use of a solution of citric acid (5 g/L), while the Italian Decree recommends a 3% (v/v) solution of acetic acid [1]. The different acids could lead to different results for the same type of material. In addition, completely different anti-corrosion behaviors can occur for the same type of material due to differences in the microstructural characteristics, such as the grain size, grain boundaries, precipitates, inclusions, and defects [12].

In these test protocols, the acceptance or rejection of a metallic material is based on the amount of metal ions released. However, the established test conditions are very specific with respect to the reaction area and electrolyte volume ratio [8]. Generally, large reaction areas and small electrolyte volumes are used, and these working conditions cause a dynamic and continuous variation of the chemical composition of the electrolyte. This is contrary to what is suggested to determine the corrosion resistance of a material, for which it has been established that the chemical composition of the electrolyte must be constant during the test period.

Since the release of metal ions into the electrolyte is mainly due to the presence of electrochemical processes, electrochemical techniques are an appropriate tool for determining which materials have greater susceptibility to metal ion release (that is, higher corrosion rates) [8]. Therefore, the objective of this study is to investigate the electrochemical behavior of different austenitic stainless steels to determine the effect of both the different alloy elements and their microstructural characteristics on the release of metal ions. The experimental conditions used were similar to those established by the Italian Decree text [11].

2. EXPERIMENTAL PROCEDURE

2.1. Materials

The austenitic stainless steels evaluated correspond to the 300 series. Table 1 shows the elemental chemical composition according to ASTM standards A213/A213M and A240/240M for

steels 304, 310, 316, 321, and 347 and according to the manufacturer for steels 303 and 330. The chemical composition was verified by X-ray energy dispersive spectroscopy (EDS), and the results agree with the reported values.

Table 1. Chemical composition of evaluated austenitic stainless steels according to ASTM A213/A213M, ASTM A240/A240M, and supplier.

Grade	Chemical composition (wt. %, Fe Balance)										
	C	Mn	P	S	Si	Cr	Ni	Mo	Nb	Ti	Cu
303	0.04-0.15	2.00	--	0.150	1.00	17.0-19.0	8.0-10.0	--	--	--	--
304	0.04-0.10	2.00	0.045	0.030	1.00	18.0-20.0	8.0-11.0	--	--	--	--
310	0.04-0.10	2.00	0.045	0.030	1.00	24.0-26.0	19.0-22.0	--	--	--	--
316	0.04-0.10	2.00	0.045	0.030	1.00	16.0-18.0	11.0-14.0	2.00-3.00	--	--	--
321	0.04-0.10	2.00	0.045	0.030	1.00	17.0-19.0	9.0-12.0	--	--	4(C+N)-0.7	--
330	0.04-0.08	2.00	0.030	0.030	1.50	18.0-22.0	34.0-37.0	--	--	--	1.00
347	0.04-0.10	2.00	0.045	0.030	1.00	17.0-19.0	9.0-12.0	--	8C-1.10	--	--

2.2. Microstructural Characterization

The microstructure of the steels was characterized. The samples were sequentially abraded with silicon carbide abrasive paper (120 to 1200), followed by polishing with diamond paste (0.25 microns). The microstructure was revealed by electrolytic etching in a solution of 10% oxalic acid (wt/v), as recommended by ASTM E407. Scanning electron microscopy (SEM) and EDS analysis were used to observe the different microstructural characteristics of the steels.

2.3. Sample Preparation

For the corrosion tests, metal samples with dimensions of 10.0x10.0x3.0 mm were sectioned. A copper wire was welded to the samples on one of their faces by spot-welding. In this condition, the samples were encapsulated in epoxy resin. Surfaces of the encapsulated samples were abraded with 120 to 1200 grit silicon carbide abrasive paper to expose the reaction area. Subsequently, the samples were washed with distilled water and ethanol, dried with hot air, and immediately immersed in electrolyte for corrosion tests.

2.4. Corrosive Medium

The test solution suggested by the Italian Decree text was used as a corrosive medium (Italian law text, 1973): 3% (v/v) acetic acid solution (pH 2.45) at 40°C. The volume of electrolyte was 200 ml (that is, the area:volume ratio was 1:200 (0.005 cm⁻¹)). This condition guarantees an insignificant variation in the corrosivity of the electrolyte according to ASTM G31.

2.5. Electrochemical Evaluation

The electrochemical behavior of the stainless steels was determined in an electrochemical cell with three electrodes. The different encapsulated steels were used as the working electrode (WE), while a saturated calomel electrode was used as a reference electrode (SCE), and a graphite bar was used as a counter electrode. The different stainless steels were subjected to tests to obtain the potentiodynamic polarization curves, open circuit potential measurements (OCP), linear polarization resistance measurements (LPR), and electrochemical impedance spectroscopy (EIS) measurements.

The potentiodynamic polarization curves were obtained by polarizing the WE from -400 to 1800 mV with respect to its corrosion potential (E_{corr}) at a scanning rate of 1 mVs^{-1} according to ASTM G3. From these measurements, E_{corr} and the corrosion current density (I_{corr}) were obtained by extrapolating the Tafel slopes in the range of $\pm 250 \text{ mV}$ around E_{corr} . OCP measurements were carried out by measuring the potential of the WE with respect to the SCE at intervals of one hour. LPR measurements were done by polarizing the WE with $\pm 10 \text{ mV}$ with respect to its open circuit potential at a scanning rate of 0.1667 mVs^{-1} at one-hour intervals. The electrochemical impedance spectra (EIS) were obtained by applying a perturbation of $\pm 10 \text{ mV}$ with respect to the open circuit potential of the WE in a frequency range of 100 kHz to 0.01 Hz.

The OCP, LPR, and EIS measurements were performed for 100 hours. In all cases, the electrochemical cell was allowed to stabilize for one hour before starting any measurement. Potentiodynamic polarization curves were obtained with a Gill AC potentiostat/galvanostat (ACM Instruments), and the OCP, LPR, and EIS measurements were obtained in an Interface 1000 potentiostat/galvanostat (Gamry).

3. RESULTS AND DISCUSSION

3.1. Microstructural Characterization

Figure 1 shows the different microstructural aspects of the austenitic stainless steels. In general, the microstructures mainly consisted of equiaxed austenite grains with annealed twins [13-14] and slight differences in grain sizes. However, the steels also showed precipitates and inclusions.

The EDS analysis indicated the presence of MnS inclusions in the 303SS, small precipitates of titanium nitride in 304SS, and a high content of chromium carbide precipitates at the grain boundaries and in the grains in 310SS. There were small precipitates of titanium nitride dispersed in the grain boundaries of 316SS, as well as precipitates from chromium carbide that were rich in Ti, S, C, and N in the grain boundaries of 321SS. There were chromium carbide precipitates in both the grain boundaries and in the grains in 330SS, and Nd, C, and S rich precipitates were observed at the limits of the grains in 347SS.

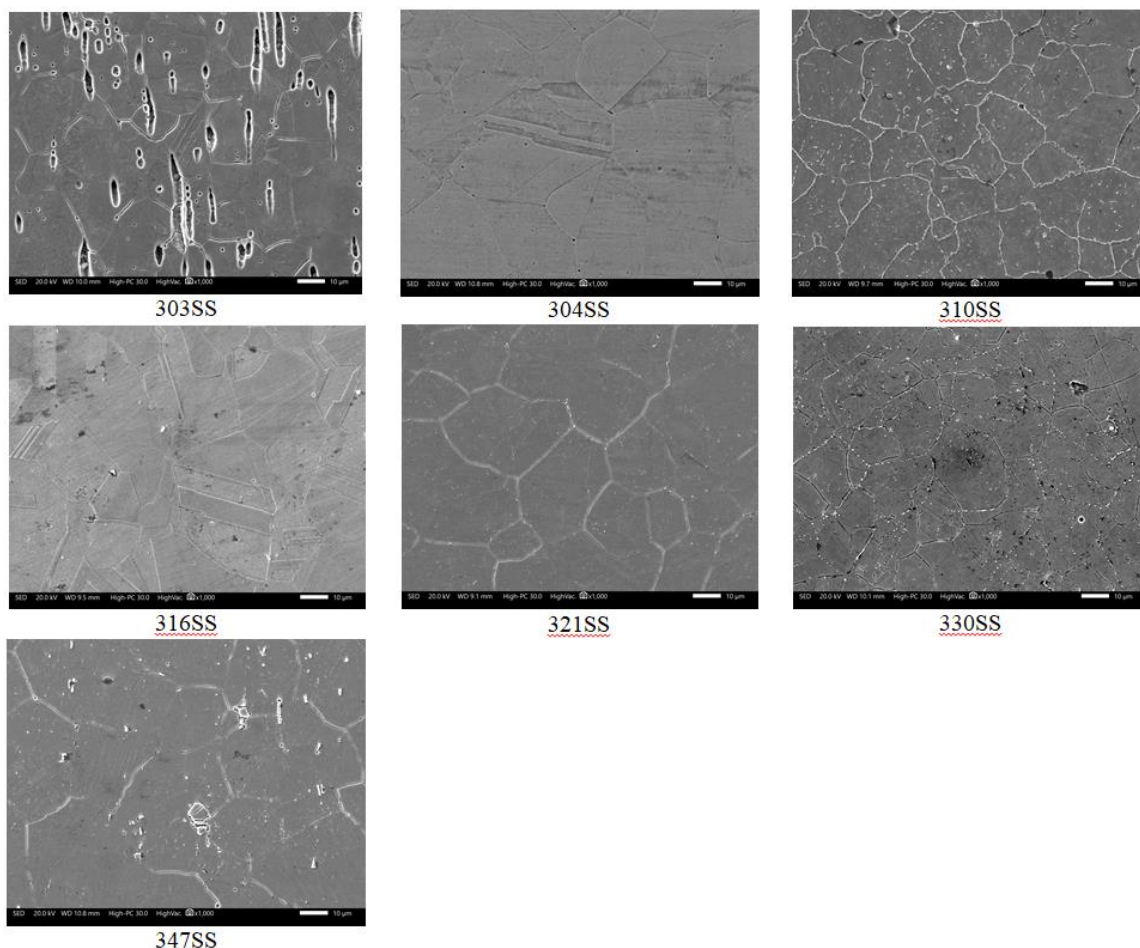


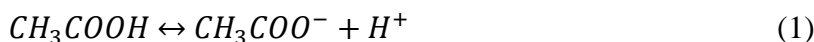
Figure 1. Microstructural aspects of different stainless steels.

In addition to the chemical composition, the microstructure characteristics can also affect the corrosion behavior of stainless steels. In general, a decrease in the grain size increases the uniform corrosion rate [15-19], decreases the intergranular corrosion [15, 18], and increases the pitting corrosion resistance [13, 15-18]. However, chromium carbide precipitates can cause a depletion of Cr in the metal matrix adjacent to the grain boundaries and increase the susceptibility to intergranular corrosion [20-24]. In addition, chromium carbide is nobler than the metal matrix, so galvanic pairs can also form [22-23]. Similar effects of galvanic corrosion can occur between the metallic matrix and the precipitates of Ti (sulfides, carbides, and nitrides) and Nb (sulfides and carbides), and the presence of MnS inclusions favors preferential dissolution in acidic environments.

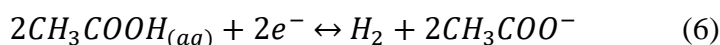
3.2. Potentiodynamic Polarization Curves

Figure 2 shows the potentiodynamic polarization curves of the different steels in acetic acid solution at 40°C. The current-potential response obtained is a function of the electrochemical reactions between the electroactive species on the metal surface, and the reaction rate depends on their concentration and mass transfer processes. It is necessary to analyze the electrolyte to understand the

observed behavior. In an aqueous solution, acetic acid dissociates according to the following expression:



However, the reaction is reversible, so the final concentration of acetic acid and acetate ion depends on the pH of the solution. According to the reaction, dissociation is favored by increasing the pH of the solution. However, around the corrosion potential (Tafel region), metal dissolution reactions occur along with two parallel cathodic reactions corresponding to the reduction of hydrogen ions and non-dissociated acetic acid:



Recent studies [25-26] indicate that acetic acid is not a significant electroactive species and it only acts as a proton-generating source on the metallic surface (dissolution reaction of acetic acid). Its contribution is only reflected as an increase in the mass transfer current limit of the cathodic current. That is, acetic acid only acts as a buffer because the cathodic reaction (reduction of H^+) promotes the dissociation of acetic acid (generation of H^+) and has no direct participation in the charge transfer process [25].

Therefore, the polarization curves show that all steels have similar behavior, which is logical because all of them are part of the 300 series. In general, their anodic behavior shows the formation of a pseudopassive zone and a posterior transpassive zone around the same potential (900 mV), independently of E_{corr} . Similar behaviors have been reported in other studies [2, 27-28]. The increase in current density around 900 mV may be due to the dissolution of the passive film or the oxidation of the electrolyte (O_2 evolution) [2]. The subsequent increase in current density (around 1300 mV) may correspond to the pitting potential. In the cathodic branches, there is a linear region just below E_{corr} that is associated with the reduction of hydrogen ions in all steels, followed by a region of mass transfer limit current (303SS, 321SS, 330SS, and 347SS).

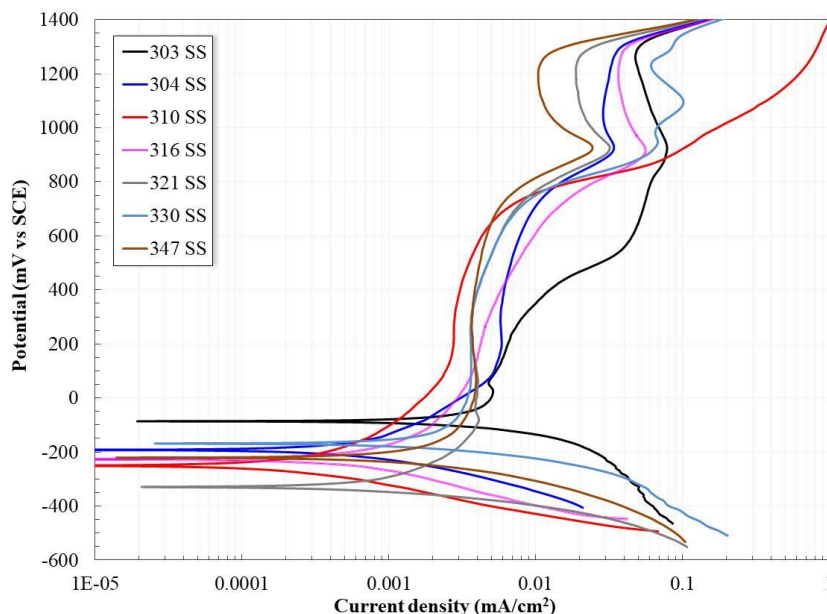


Figure 2. Polarization curves for stainless steel in acetic acid solution (3% v/v HAc) at 40°C.

A normalization of the potential values and a magnification of the Tafel region (Figure 3) show that all steels exhibit a tendency toward passivation at values slightly above their corrosion potential. The graph shows that the I_{corr} are within the same order of magnitude. The steel with the highest Cr content (310SS) develops a pseudopassive zone at lower current densities, and the steels with similar Cr content develop pseudopassive zones around the same current density value except for 303SS, which develops the zone at higher current densities. This may possibly be due to its high content of MnS inclusions.

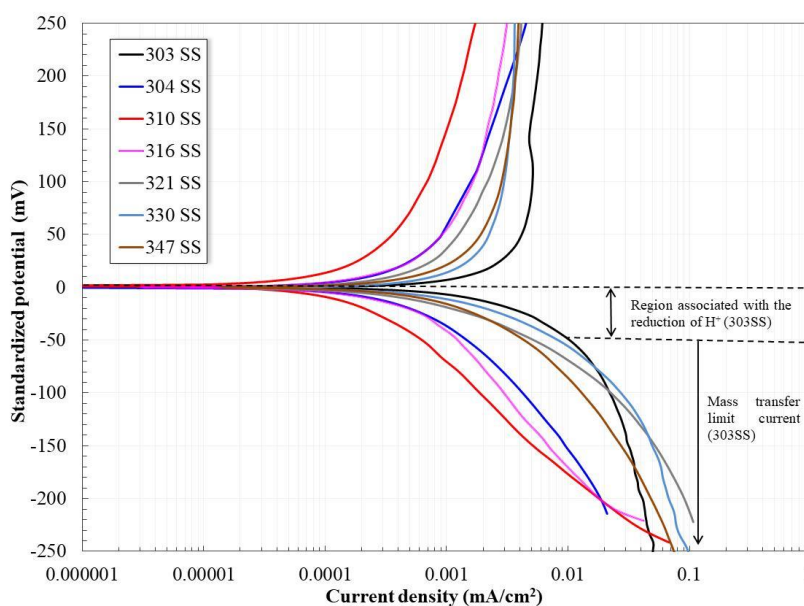


Figure 3. Normalized polarization curves and magnification of the Tafel region.

The steel with the highest Cr content (310SS) develops its cathodic branch at the lowest current densities, followed by 304SS and 316SS. Other steels with a high content of precipitates or inclusions show higher cathodic current densities and a tendency to develop a mass transfer limit current zone. This is supported by Kahyarian [26], who indicate that the cathodic reaction rate is constant at a constant pH, and therefore, an increase in the cathodic current density suggests both an increase in the reduction rate of the acetic acid and the development of a mass transfer limit current. In this sense, 303SS and 330SS clearly develop a mass transfer limit current.

Based on the electrochemical parameters obtained from the polarization curves (Table 2), it is possible to determine which materials have the best corrosion resistance characteristics. For example, materials with more active E_{corr} will show a greater tendency to corrode, while materials with a tendency toward passivation show a greater b_a value than b_c , and those with the lowest I_{corr} show the best performance against corrosion [19]. These criteria are easy to interpret when there are significant differences in I_{corr} and when the electrochemical behavior of the alloy depends on only the chemical composition, considering that all the elements are in solid solution. However, the interpretation of the electrochemical parameters is not simple when it is difficult to meet these criteria and the thermomechanical history of the materials is different or unknown. Thus, correlations were obtained for the electrochemical parameters of the steels with their chemical composition and microstructural characteristics.

Table 2. Electrochemical parameters of steels evaluated in acetic acid solution at 40 °C.

Stainless Steel	E_{corr} (mV)	b_a (mV/Dec)	b_c (mV/Dec)	I_{corr} (mA/cm ²)
303	-85	1745	495	0.00485
304	-193	342	140	0.00084
310	-250	511	124	0.00056
316	-227	541	140	0.00114
321	-329	532	105	0.00158
330	-167	968	225	0.00236
347	-222	999	161	0.00233

The behavior of 304SS and 310SS was considered as a reference because their minor element contents are similar, and their Cr and Ni contents are different. Figure 4 shows that increasing both the Cr and Ni contents makes the E_{corr} more active. Furthermore, Ti, Mo, and Nb also make E_{corr} more active, and the addition of S and Si makes the E_{corr} values nobler. This behavior was not expected since the steel should show a lower tendency to corrode (the noblest potential) with higher Cr content. This can be explained based on the studies by Kahyarian [26]. They indicated that in corrosion processes with acetic acid, the corrosion potential can be affected by the cathodic reaction rate (the reduction of H^+). Therefore, when increasing the Cr and Ni concentrations, there is a decrease in the cathodic reaction rate and thus the corrosion rate (304SS and 310SS).

However, the other steels do not follow this trend. In the case of 303SS and 330SS, the E_{corr} values are nobler. In this sense, Kahyarian [26] also indicate that an increase in E_{corr} is due to the rapid consumption of protons (an increase in the cathodic reaction rate), which results in a mass transfer limit current. Figure 3 shows that these two steels developed a limit current in the cathodic branch. However, in the case of 316SS, 321SS, and 347SS steels, E_{corr} was more active. Thus, it seems that E_{corr} is associated with the additional alloying elements (Mo, Ti, and Nd) or precipitates in the microstructure rather than the cathodic reaction rate.

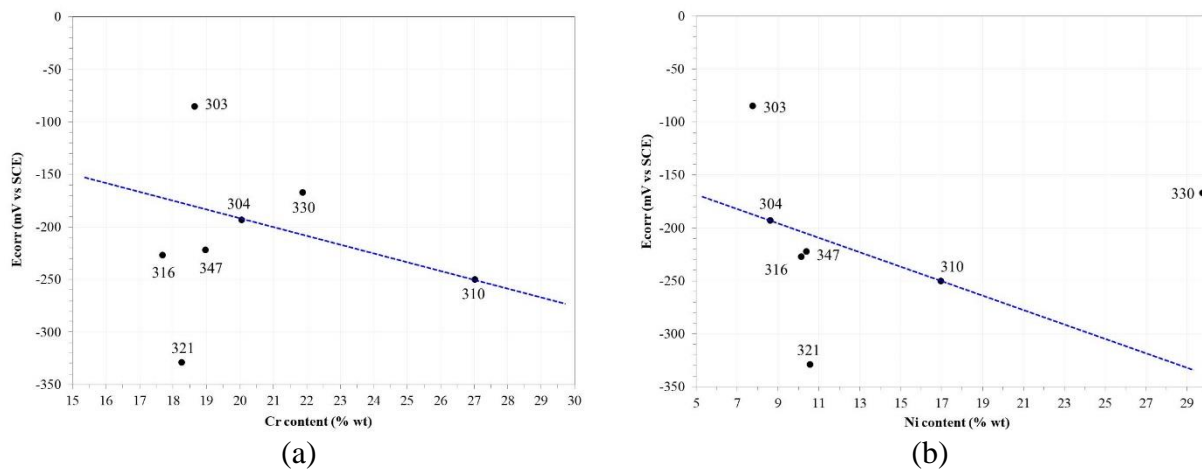


Figure 4. Effect of the Cr (a) and Ni (b) content on the corrosion potential of stainless steels.

Figure 5 shows that an increase in the Cr and Ni content contributes to reduce the corrosion rate (304SS and 310SS). However, the other steels (303SS, 316SS, 321SS, 330SS, and 347SS) show deviations from this behavior; that is, I_{corr} is higher than expected for similar Cr or Ni contents. It is clear that other alloying elements or precipitates had a detrimental effect on the corrosion resistance of the steels. In the case of precipitated phases, metal dissolution is favored due to the formation of galvanic pairs or points of initiation of pitting attack [29-30].

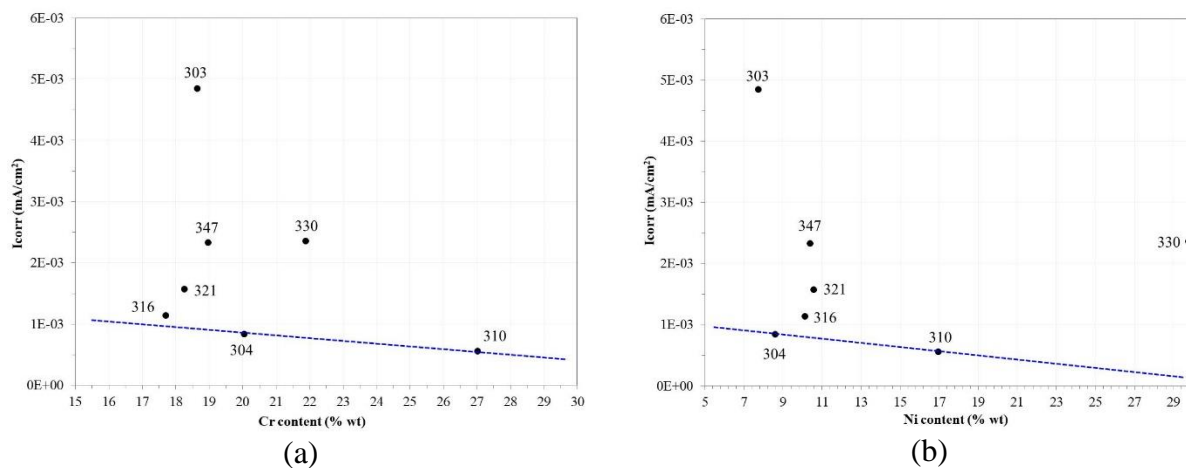


Figure 5. Effect of Cr (a) and Ni (b) content on the I_{corr} values of stainless steels.

Figure 6 shows the effect of the anodic slope on the cathodic slope relationship with the I_{corr} values. A material with an anodic slope that is greater than its cathodic slope will show a greater tendency to passivate; otherwise, the material will have a greater tendency to corrode [19]. An excellent correlation is observed between steels with similar Cr content (18-20%). This shows that the presence of Mo, Ti, Nb, or their precipitates increases the corrosion tendency of the steel. Furthermore, the addition of S or Cu or inclusions of MnS accelerates the corrosion rate. In addition, the steel shows a lower tendency to corrode when increasing the Cr content (310SS).

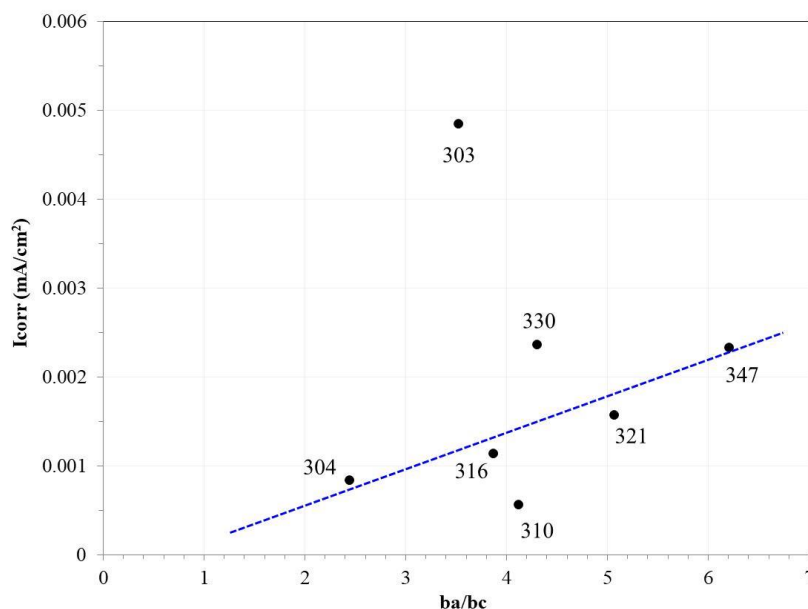


Figure 6. Effect of the ba/bc relationship on the I_{corr} value of stainless steels.

3.3. Open Circuit Potential Measurements

Figure 7 shows the variation in the OCP values of the stainless steels in acetic acid solution at 40°C for 100 hours. OCP is mainly a function of the chemical composition of the steel, but other variables can also affect it, such as the thermomechanical history of the alloy, the composition of the electrolyte, temperature, and the flow of the solution [12]. All steels exhibited a shift in the OCP in the noble direction. This agrees with the polarization curves, where all steels showed a rapid tendency to passivate at values slightly above E_{corr} .

Some steels tended to rapidly reach steady state (316SS), and others showed an active behavior at the beginning of the test (303SS), followed by an increase in the OCP until reaching a pseudo-stationary trend. The other steels showed a constant increase in the OCP without reaching a definite steady state. According to the position of the OCP curves, the corrosion tendency of the steels increases in the following order: 303SS > 330S > 316SS > 321SS > 347SS > 310SS > 304SS. In general, the corrosion resistance of stainless steels is due to the rapid development of a thin passive film of about 1-3 nm in thickness. Its protective characteristics depend on its Cr content, with higher Cr content in the alloy resulting in higher Cr content in the passive film. This occurs because the

selective dissolution of the other alloying elements is suppressed, and the oxidation of the Cr of the alloy is favored [31].

However, the trends do not follow these considerations. Therefore, it is possible that the observed behavior is associated with the microstructural characteristics (grain size, precipitates, or inclusions) or alloying elements such as Cu, Mo, Ti, Nb, Si, and a higher content of S. For example, 310SS has a higher Cr content than 304SS, but its OCP is more active. The rest of the steels have similar Cr content to that of 304SS, and their behavior was more active than that observed for 304SS.

In the case of 310SS, the behavior could be due to the high content of Cr carbide precipitates. As already indicated, the precipitation of chromium carbides causes a Cr depletion in the metal matrix [20-24] and favors the formation of galvanic pairs [22-23]. The most active behavior was observed in 303SS, which may have been due to the preferential dissolution of MnS inclusions, which caused an increase in the reaction area of the steel [3, 12, 24, 31]. Precipitates and Cu also increase the metal dissolution rate [24].

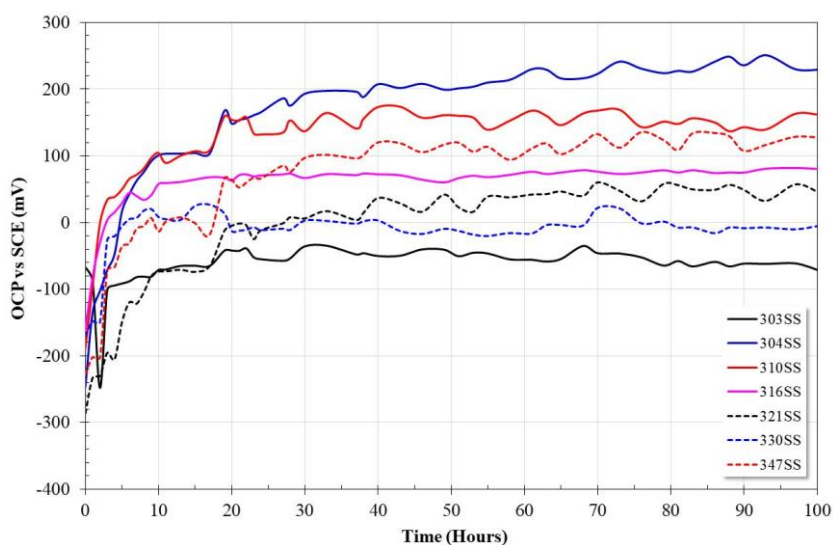


Figure 7. Variation of OCP as a function of time for stainless steels immersed in acetic acid solution at 40°C.

3.4. Linear Polarization Resistance Measurements

Figure 8 shows the variation of the polarization resistance of the stainless steels in acetic acid solution at 40°C for 100 hours. All stainless steels showed high corrosion resistance with R_p values greater than 1×10^5 ohms/cm². However, the particular tendencies and values were different and appear to depend on the chemical composition, or precipitates, or inclusions in the microstructure.

With the exception of 303SS, the stainless steels showed a rapid initial increase in R_p (with immersion times less than 10 hours), followed by a quasi-stationary trend or constant increase of the resistance. In the case of 303SS, the initial drop in R_p could be associated with the rapid dissolution of MnS inclusions. Other studies have reported this phenomenon for the same type of steel in acetic acid

solutions [3, 24] and acidic solutions in general [12, 31]. In addition, MnS inclusions can be nucleation points for pitting [12, 31].

The subsequent increase in its R_p corresponds to the formation of a protective passive layer, but values are the lowest due to the increase in the reaction area as a consequence of the large number of cavities caused by the dissolution of the MnS inclusions. Both 304SS and 310SS showed the highest R_p . 310SS had the highest Cr content, but 304SS was the only steel with practically no precipitates visible in its microstructure. In the case of 316SS, 321SS, 330SS, and 347SS steels, the Cr contents were similar to that of 304SS, but the resistance were lower. Again, it seems that Mo, Ti, Cu, Si, Nb, or precipitates result in a decrease in the corrosion resistance of the steels.

This can be interpreted as an increase in the corrosion current density due to the galvanic pairs generated between the precipitates and the metal matrix. Alternatively, it could be due to a decrease in the Cr content of the metal matrix as a consequence of the formation of chromium carbide precipitates. Based on the polarization resistance tests, the metal dissolution of the steels varied in the following order: 303SS > 316SS > 321SS \approx 330SS > 347SS > 310SS \approx 304SS. In addition, the highest release of metal ions occurred in the first 10 hours of testing except for 303SS, which showed an appreciable release of metal ions until 24 hours of immersion. The trends of R_p indicate the formation of a stable protective oxide enriched in Cr, which minimizes the metallic dissolution of the steel [6].

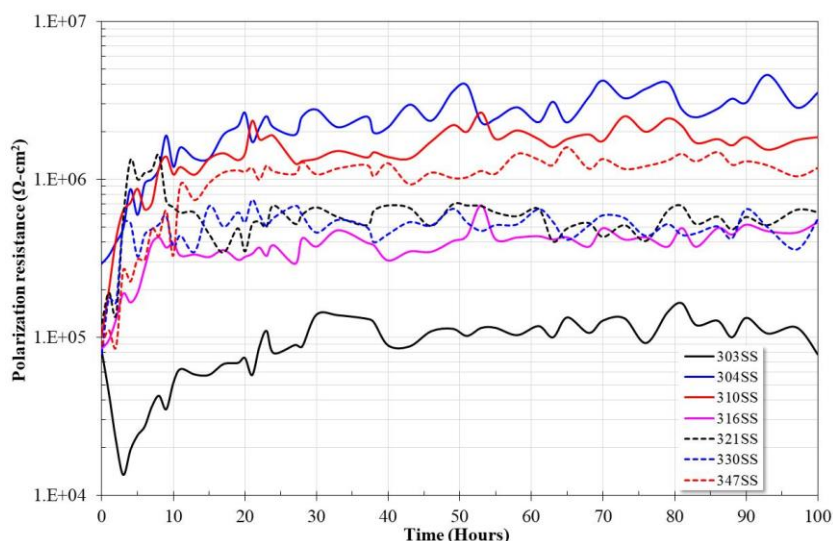


Figure 8. Variation in the polarization resistance as a function of time for stainless steels immersed in acetic acid solution (3% v/v) at 40°C.

Typical corrosion tests for materials that come in contact with simulated food fluids are based on the amount of metal ions that are released into the electrolyte. The concentration of metal ions released increases when increasing the ratio between the reaction area and the electrolyte volume (A/V) [5, 8]. Considering a constant corrosion rate, the amount of metal ions released per unit volume will always be greater for small volumes of electrolyte (large A/V ratio); that is, there is a concentration effect of the metal ions. Due to the complexing capacity of the acetate ions, metal acetates form, so the equilibrium of the reaction (1) shifts in favor of the dissociation of acetic acid and

increases the release of protons. This suggests that at large A/V ratios, in addition to a concentration effect of metal ions, the dissociation of acetic acid depends on not only the cathodic reaction rate (reaction 5), but also the formation of metallic acetates, which are highly stable under acidic conditions [32, 33]. Therefore, this additional dissociation of acetic acid can increase the corrosivity of the electrolyte.

3.5. Electrochemical Impedance Spectroscopy Measurements

Figure 9 shows the impedance spectra in Nyquist and Bode format after 100 hours of testing. In the Nyquist diagram, all steels showed the formation of a capacitive semicircle. The trends indicate that 304SS and 310SS have the highest charge transfer resistance, followed by 347SS, 330SS, 321SS, 316SS, and 303SS. It is not possible to observe more characteristics of the corrosion process because the information observed in the Nyquist diagrams generally corresponds to approximately 30% of the total experimental data. Most of the experimental data correspond to the low frequency region (less than 1-10 Hz). Therefore, analyzing the impedance spectra based on the Bode diagrams is the best way to analyze the information obtained from the whole range of frequencies evaluated.

Based on the impedance module of the Bode diagram, $|Z|$, all steels developed a high frequency plateau (> 1000 Hz), which determines the electrolyte resistance. The plateau began to develop at frequencies greater than 100 Hz. This plateau allows us to establish that there was no formation of a layer of corrosion products layer that was adsorbed onto the metal surface.

In the intermediate frequency region, which is generally located between 1-10 Hz and 1000 Hz, there is linear relationship $\log |Z| - \log f$, which establishes the capacitive properties of the metal surface. This region shows a linear relationship with two apparent slopes. In the low frequency range ($< 1-10$ Hz), a low-frequency plateau did not form, which indicates that the charge transfer resistance is greater than the last $|Z|$ value recorded. The trend of $|Z|$ in the low-frequency region coincides with that observed in the Nyquist diagram.

The phase angle format of the Bode diagram, ($^\circ$), shows that the phase angle tends to zero from 100 Hz in the high-frequency region. This coincides with the formation of a high-frequency plateau and indicates the absence of a corrosion product layer adsorbed onto the metal surface. The intermediate-frequency region, where the capacitive properties of the metallic surface are observed, extends to frequencies lower than 0.01 Hz. In this region, there are two phase angle maxima, which indicate two time constants. The first one is between 1 and 10 Hz, and the second one is around 0.1 Hz. The first time constant shows a lower phase angle than the second one. Both the charge transfer resistance and the impedance modulus of the steels coincide with the order of the maximum phase angle of the second time constant.

It can be inferred that the steels developed a thin passive film with excellent capacitive properties according to the impedance spectra, including (i) the high frequency plateau as well as its development from frequencies below 1000 Hz, (ii) the absence of a low-frequency plateau, and (iii) time constants with phase angles up to 80° .

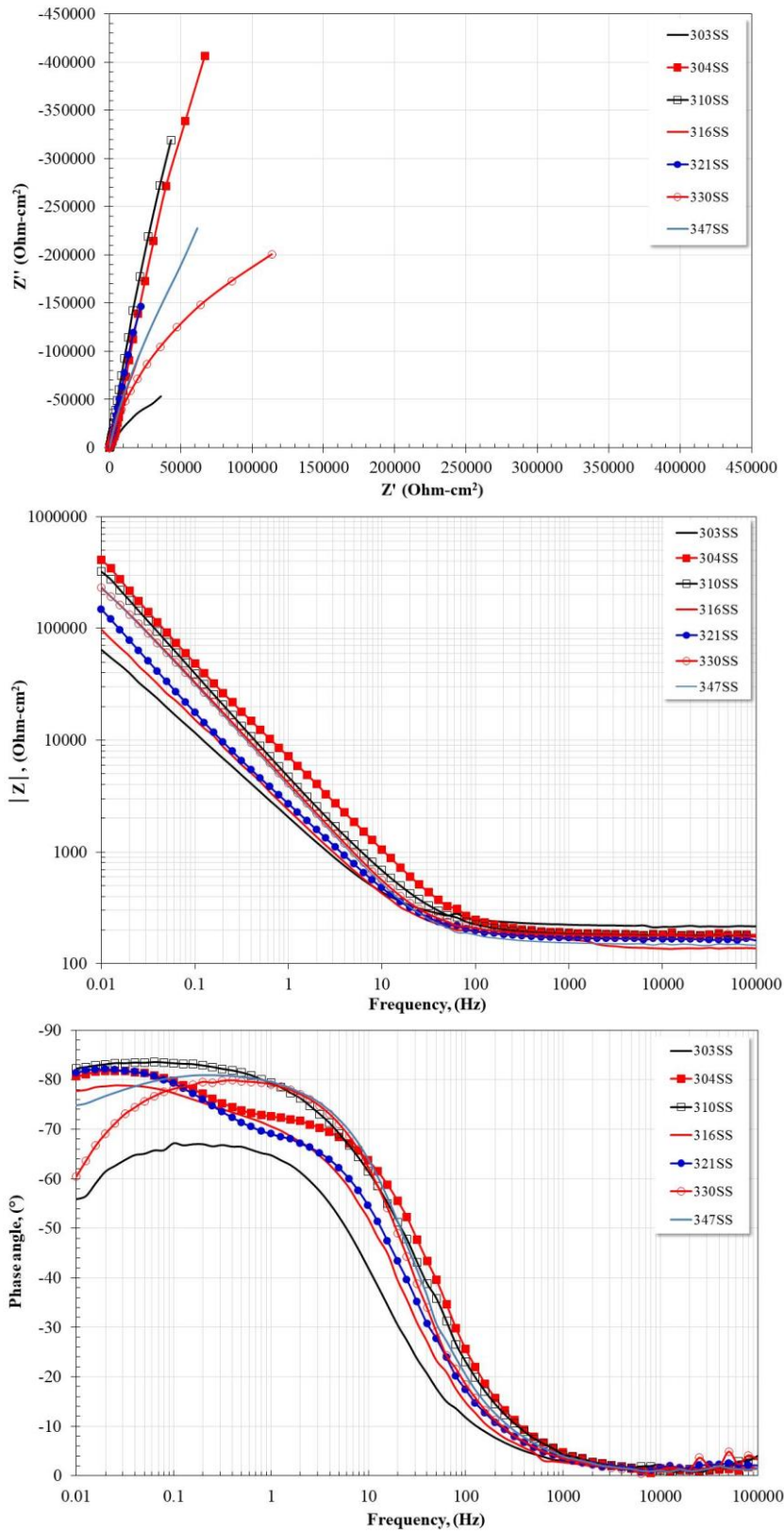
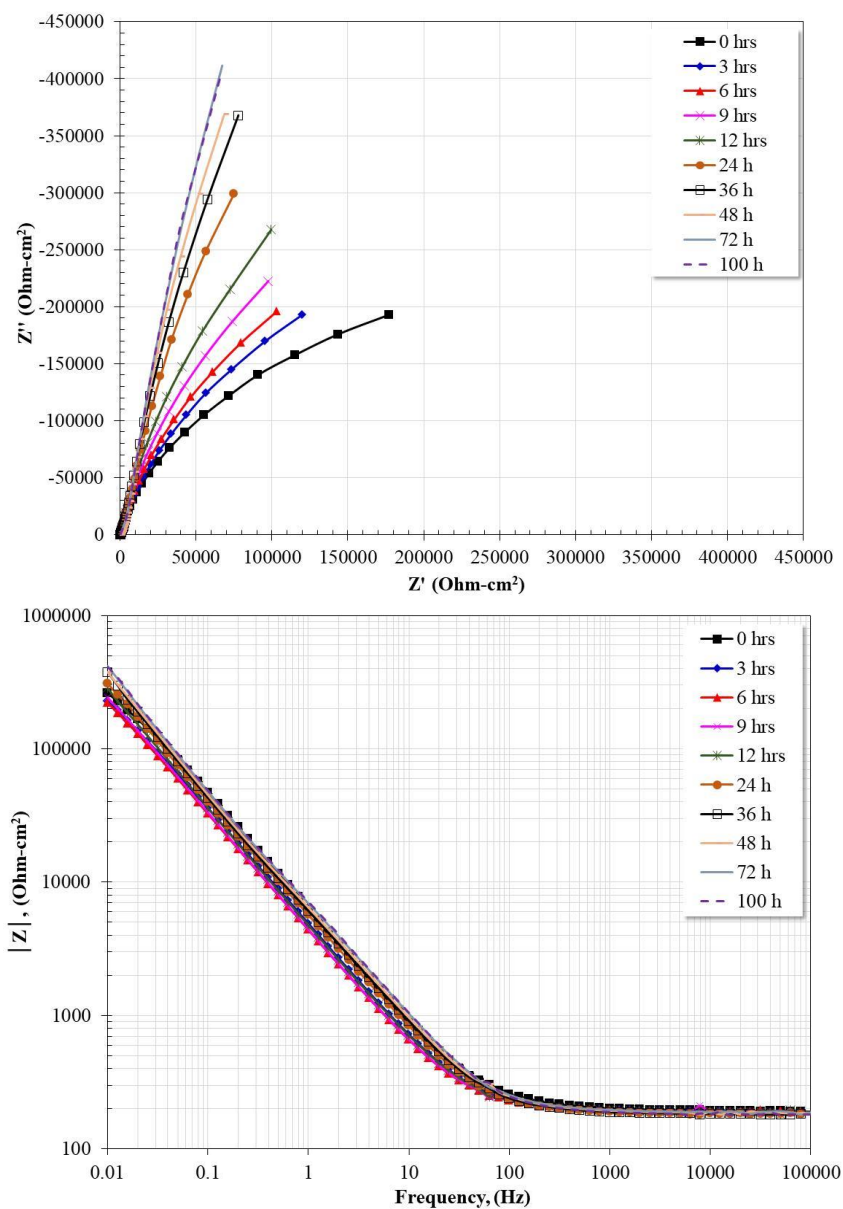


Figure 9. Nyquist and Bode diagrams for austenitic stainless steels after 100 hours of immersion in acetic acid solution at 40°C.

In general, the passive films on the stainless steels are 1-3 nm thick, and their capacitive properties depend on the Cr content [31]. Based on the similarity between the different spectra, qualitatively, it can be established that the same surface processes occur on the surface of the steels, and the differences are a function of the microstructural characteristics and chemical composition [28].

Figure 10 shows the variation of the impedance spectra as a function of time for 304SS. The behavior was similar to the other steels. The Nyquist diagram shows a single apparent capacitive semicircle with constantly increasing diameter as a function of the immersion time. This indicates a constant increase in the charge transfer resistance.



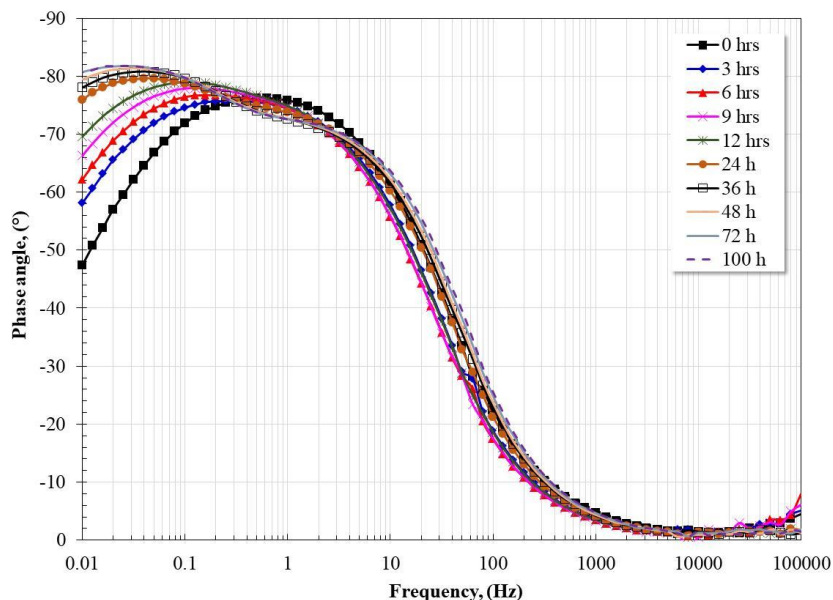


Figure 10. Variation of Nyquist and Bode diagrams with respect to immersion time for 304SS in acetic acid solution at 40°C.

The observed information only corresponds to a part of the electrochemical behavior of the steel because the remaining information is suppressed by the high resistance of the steel. The same characteristics observed before occur in the Bode diagram in its impedance module format, $|Z|$, in both the high-frequency and intermediate-frequency regions. In the low-frequency region, large values of the impedance modulus are observed and tend to increase as a function of the immersion time. The absence of a low-frequency plateau indicates that the impedance module are greater than the last registered value.

The same characteristics as before were again observed in the high-frequency region of the Bode diagram in its phase angle format, ($^{\circ}$). At time zero, from the intermediate-frequency region to the low-frequency region, there are two overlapping time constants with a maximum angle of 76° around 0.5 Hz. At longer immersion times, the two time constants separate. The first one shifts slightly to higher frequencies (around 2-3 Hz) with a slight decrease in its maximum phase angle (around 71°), while the second one shifts to the low-frequency region, and its maximum phase angle increases to 81° . The impedance spectra were fitted with the equivalent circuit shown in Figure 11, which is suggested for modeling impedance spectra of materials that develop passive films on their surfaces [34-36].

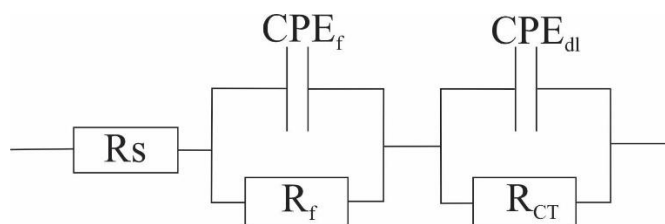


Figure 11. Equivalent circuit used for modeling the impedance spectra.

R_s is the solution resistance, CPE_{dl} is the constant phase element (CPE) of the electrochemical double layer, R_{ct} is the charge transfer resistance, R_f is the resistance of the protective film, and CPE_f is the constant phase element of the protective film. The capacitance generally does not show ideal capacitive behavior, so it is suggested that CPE be used to compensate for the dispersion effect caused by the roughness of the electrode interface. The impedance of the CPE is determined by the following expression [37]:

$$Z_{CPE} = \left(\frac{1}{Y_0}\right) (j\omega)^{-n}$$

where Y_0 is the constant magnitude of the CPE ($F\ cm^{-2}\ s^{(n-1)}$), ω is the angular frequency ($rad\ s^{-1}$), $j^2 = -1$ is the imaginary number, and n is a phenomenological coefficient that indicates the phase shift and represents the heterogeneity of the surface ($0 < n < 1$). If $n = 1$, $CPE = C = 1/Y_0$, while if $n = 0.5$ $CPE = Z_w$ (Warburg impedance), and if $n = 0$ $CPE = R$. The capacitance of the CPE can be calculated using the following equation [38]:

$$C_{CPE} = \frac{(Y_0 R_f)^{1/n}}{R_f}$$

Figures 12 to 14 show the variation of the fit parameters obtained from the modeling of the impedance spectra. Figure 12 shows the variation of the R_{ct} and R_f values. The figures show great similarity in the values and trends of R_{ct} to the measurements of the polarization resistance (R_p). This indicates that the equivalent circuit adequately represents the surface processes occurring on the working electrodes. The possible differences could be due to the fact that in general, $R_p \approx R_{ct} + R_f$. It can be said that R_c varies according to the variation of R_p .

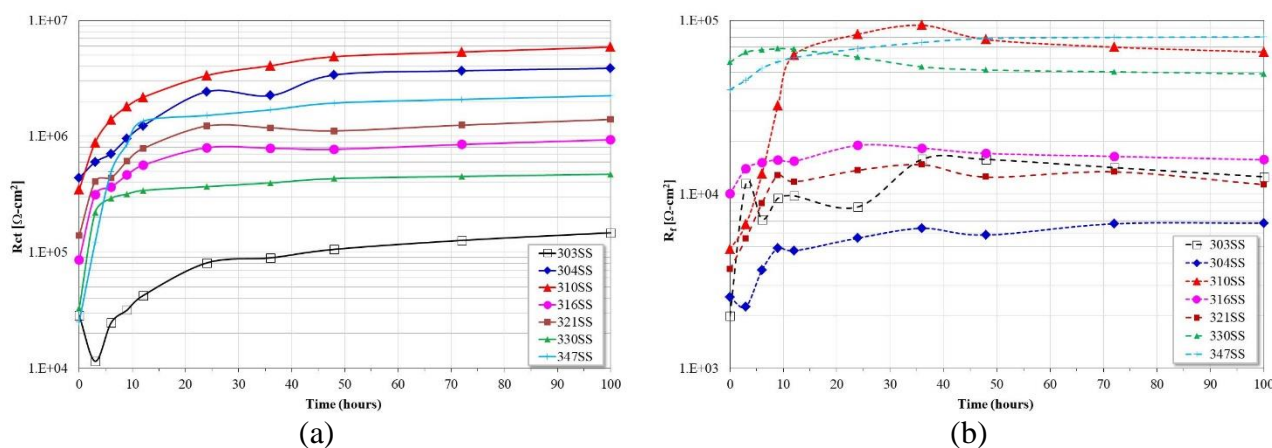


Figure 12. Variation of R_{ct} and R_f as functions of time.

According to the graph, the steels with the greatest corrosion resistance are $304SS \approx 310SS$, and 303SS had the lowest corrosion resistance. However, the R_f values show differences, and the

highest values are observed for 321SS, 330SS, and 347SS, while 304SS had the lowest. The differences in R_f could be associated with either the passive film thickness or the degree of Cr enrichment.

Figure 13 shows the variation of n_{ct} and n_f . n_{ct} is greater than n_f and generally greater than 0.9. This behavior is close to an ideal electrochemical double layer capacitor. The differences observed in n_f could be associated with either the degree of Cr enrichment of the passive films or superficial defects.

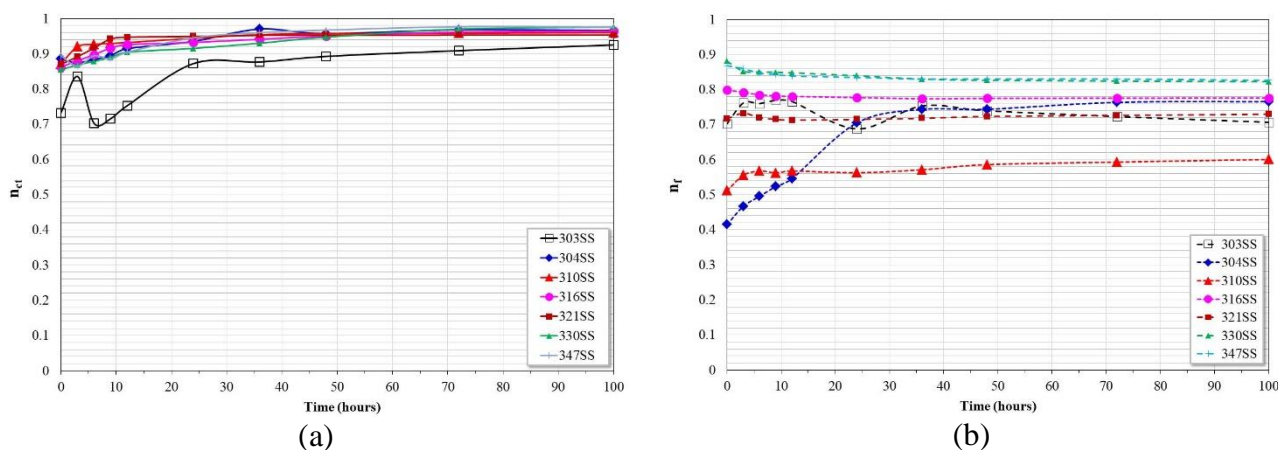


Figure 13. Variation of n_{ct} and n_f as functions of time.

Figure 14 shows the variation of C_{dl} and C_f . For all steels, C_{dl} decreases rapidly in the first hours of immersion, and then the tendency is less pronounced until it reaches a quasi-stationary state at longer times.

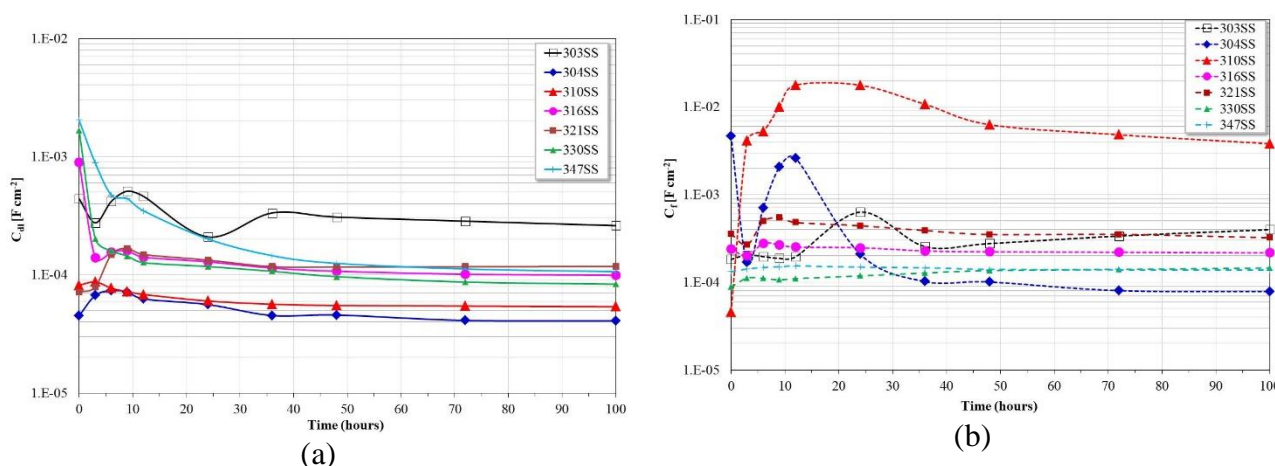


Figure 14. Variation of C_{ct} and C_f as functions of time.

This constant decrease in C_{dl} is directly related to the increase in the corrosion resistance of the steels; that is, there is less current exchange at the interfaces. 304SS and 310SS showed the lowest C_{dl} ,

and 303SS showed the highest values. Regarding C_f , the steels showed fluctuations at the beginning of the test until reaching a quasi-stationary state after 40 hours of immersion. 310SS showed the highest C_f , and 304SS had the lowest one. Considering that the passive film is mainly composed of Cr_2O_3 , the variations could be associated with variations in the thickness [39-40] or the formation of a rough or porous surface that increases the surface area [41].

3.6. Morphological Analysis of Corroded Surfaces

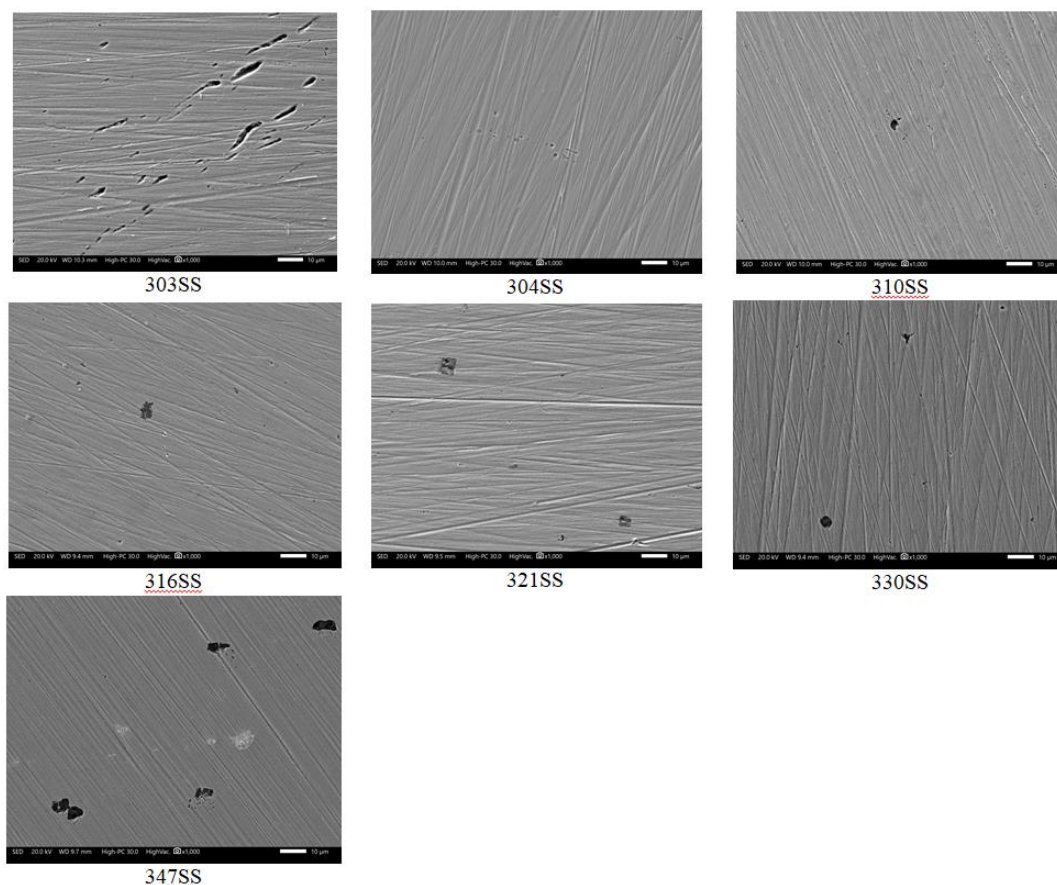


Figure 15. Morphological aspects of the austenitic stainless steels after 100 hours of immersion in acetic acid solution at 40°C.

Figure 15 shows the different surface aspects of the steels after the corrosion test in acetic acid solution at 40°C for 100 hours. In general, all the materials presented a superficial pitting attack. A detailed analysis indicates that the pitting is due to the detachment or dissolution of precipitates or inclusions. Figure 16 shows the corroded surface of 310SS and its mapping of Cr. The small pores or voids are due galvanic corrosion generated around the precipitates and the low corrosion resistance of the adjacent metal matrix because of the low Cr content as a consequence of the formation of the precipitates. Both processes caused the dissolution of the metallic matrix around the precipitates and their subsequent detachment. According to the results, both the microstructural aspects and the chemical composition of the steels have strong effects on the corrosion performance and thus the release of metal ions into the electrolyte.

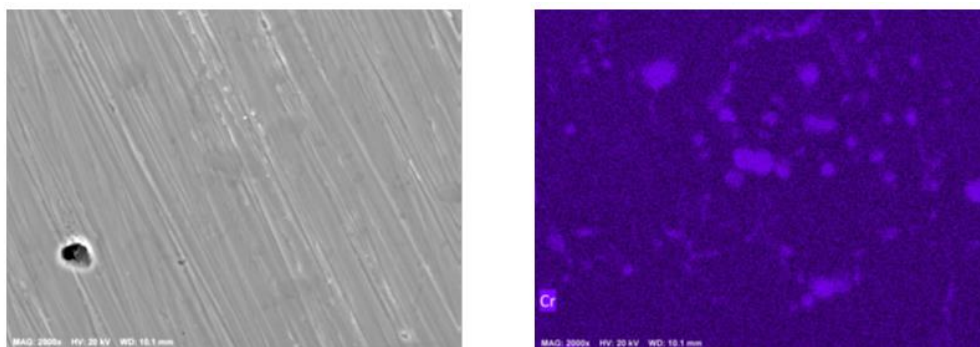


Figure 16. Surface aspect and Cr mapping of 310SS after the corrosion test.

4. CONCLUSIONS

The electrochemical performance of different austenitic stainless steels showed that both the chemical composition and the microstructural characteristics affect the resistance to corrosion and thus the ability to release metal ions into the electrolyte. The steels with precipitates or inclusions showed the highest corrosion rates. The analysis of the polarization curves showed that by increasing I_{corr} , results in greater dissociation of acetic acid, which results in the appearance of a mass transfer limit current in the cathodic branch.

Electrochemical evaluations showed that steels with higher I_{corr} , nobler OCP, higher R_p , and higher R_{ct} had higher chromium content or fewer precipitates or inclusions in the microstructure. Precipitates and inclusions favor the formation of galvanic pairs that increase the corrosion rate of the steel. In addition, higher corrosion rates and a greater release of metallic ions occurred in the first 10 hours of testing. The steels developed a thin passive film with excellent capacitive properties, and according to the modeling of the impedance spectra, the capacitive properties depend on both the degree of Cr enrichment and on its thickness.

CONFLICTS OF INTEREST

The authors declare that there are no conflicts of interest regarding the publication of this paper.

ACKNOWLEDGMENTS

K. Zuñiga-Diaz is thankful to the National Council for Science and Technology of Mexico (CONACyT) for the scholarship granted to carry out her Master's degree studies. The authors are grateful for the comments and support provided by M. Casales-Diaz and J.J. Ramos-Hernandez.

References

1. N. Mazinianian, G. Herting, I.O. Wallinder and Y. Hedberg, *Corrosion*, 72 (2016) 775. <https://doi.org/10.5006/2057>.
2. V. Shankar Rao and L.K. Singhal, *Corrosion*, 66 (2010) 085004-1. <https://doi.org/10.5006/1.3479954>.

3. R. Dalipi, L. Borgese, A. Casaroli, M. Boniardi, U. Fittschen, K. Tsuji and L.E. Depero, *J. Food Eng.*, 173 (2016) 85. <https://doi.org/10.1016/j.jfoodeng.2015.10.045>.
4. F. Guarneri, C. Costa, S.P. Cannavò, S. Catania, G.D. Bua, C. Fenga and G. Dugo, *Contact Dermatitis*, 76 (2016) 40. <https://doi.org/10.1111/cod.12692>.
5. K.L. Kamerud, K.A. Hobbie and K.A. Anderson, *J. Agric. Food Chem.*, 61 (2013) 9495. <https://doi.org/10.1021/jf402400v>.
6. G. Herting, I.O. Wallinder and C. Leygraf, *J. Food Eng.*, 87 (2008) 291. <https://doi.org/10.1016/j.jfoodeng.2007.12.006>.
7. Y.S. Hedberg and I.O. Wallinder, *Biointerphases*, 11 (2016), 018901. <https://doi.org/10.1116/1.4934628>.
8. N. Mazinianian, I.O. Wallinder and Y. Hedberg, *J. Food Eng.*, 145 (2015) 51. <https://doi.org/10.1016/j.jfoodeng.2014.08.006>.
9. A. Sandoval-Amador, J.E. Torres-Ramirez, D.Y. Vargas-Castro, J.R. Caceres-Nuñez, H.A. Estupiñan-Duran and D.Y. Peña-Ballesteros, *Matéria (Rio J.)*, 23 (2018) e-11959. <http://dx.doi.org/10.1590/s1517-707620170001.0295>.
10. CoE, 2013. Council of Europe, ISBN: 978-92-871-7703-2. *European Directorate for the Quality of Medicines & HealthCare (EDQM)*.
11. Italian law text, 1973. *Decreto ministeriale* 21/03/1973.
12. S. Schilling, A. Janssen, N.J. Zaluzec and M.G. Burke, *Microsc. Microanal.*, 23 (2017) 741. <https://doi.org/10.1017/S1431927617012314>.
13. A.S. Hamada, L.P. Karjalainen and M.C. Somani, *Mater. Sci. Eng. A*, 431 (2006) 211. <https://doi.org/10.1016/j.msea.2006.05.138>.
14. L. Jinlong and L. Hongyun, *Appl. Surf. Sci.*, 263 (2012) 29. <https://doi.org/10.1016/j.apsusc.2012.08.058>.
15. M. Hasegawa and M. Osawa, *Corrosion*, 40 (1984) 371. <https://doi.org/10.5006/1.3593940>.
16. S.V. Muley, A.N. Vidvans, G.P. Chaudhari and S. Udainiya, *Acta Biomater.*, 30 (2016) 408. <https://doi.org/10.1016/j.actbio.2015.10.043>.
17. A.A. Aghuy, M. Zakeri, M.H. Moayed and M. Mazinani, *Corrosion Sci.*, 94 (2015) 368. <https://doi.org/10.1016/j.corsci.2015.02.024>.
18. A. Di Schino and J.M. Kenny, *J. Mater. Sci. Lett.*, 21 (2002) 1631. <https://doi.org/10.1023/A:1020338103964>.
19. B.N. Mordyuk, G.I. Prokopenko, M.A. Vasylyev and M.O. Iefimov, *Mater. Sci. Eng. A*, 458 (2007) 253. <https://doi.org/10.1016/j.msea.2006.12.049>.
20. K. Kaneko, T. Fukunaga, K. Yamada, N. Nakada, M. Kikuchi, Z. Saghi, J.S. Barnard and P.A. Midgley, *Scr. Mater.*, 65 (2011) 509. <https://doi.org/10.1016/j.scriptamat.2011.06.010>.
21. J.-Y. Maetz, T. Douillard, S. Cazottes, C. Verdu and X. Kléber, *Micron*, 84 (2016) 43. <https://doi.org/10.1016/j.micron.2016.01.007>.
22. J. Qian, C. Chen, H. Yu, F. Liu, H. Yang and Z. Zhang, *Corrosion Sci.*, 111 (2016) 352. <https://doi.org/10.1016/j.corsci.2016.05.021>.
23. S. Zhang, Z. Jiang, H. Li, H. Feng and B. Zhang, *J. Alloy. Compd.*, 695 (2017) 3083. <https://doi.org/10.1016/j.jallcom.2016.11.342>.
24. G. Herting, D. Lindström, I.O. Wallinder and C. Leygraf, *J. Food Eng.*, 93 (2009) 23. <https://doi.org/10.1016/j.jfoodeng.2008.12.019>.
25. T. Tran, B. Brown, S. Nešić and B. Tribollet, *Corrosion*, 70 (2013) 223. <https://doi.org/10.5006/0933>.
26. A. Kahyarian, A. Schumaker, B. Brown and S. Nesic, *Electrochim. Acta*, 258 (2017) 639. <https://doi.org/10.1016/j.electacta.2017.11.109>.
27. Z. Feng, X. Cheng, C. Dong, L. Xu and X. Li, *Corrosion Sci.*, 52 (2010) 3646. <https://doi.org/10.1016/j.corsci.2010.07.013>.

28. E.E. Oguzie, J. Li, Y. Liu, D. Chen, Y. Li, K. Yang and F. Wang, *Electrochim. Acta*, 55 (2010) 5028. <https://doi.org/10.1016/j.electacta.2010.04.015>.
29. N. Hara, K. Hirabayashi, Y. Sugawara and I. Muto, *Int. J. Corrosion*, vol. 2012, Article ID 482730, 6 pages, 2012. <http://dx.doi.org/10.1155/2012/482730>.
30. J. Porcayo-Calderon, M. Casales-Diaz, V. M. Salinas-Bravo and L. Martinez-Gomez, *Bioinorg. Chem. Appl.*, Volume 2015, Article ID 930802, 14 pages. <http://dx.doi.org/10.1155/2015/930802>.
31. R.K. Gupta and N. Birbilis, A review, *Corrosion Sci.*, 92 (2015) 1. <https://doi.org/10.1016/j.corsci.2014.11.041>.
32. J.E. Tackett, *Appl. Spectrosc.*, 43 (1989) 490. <https://doi.org/10.1366/0003702894202986>.
33. M.I. Boyanov, K.M. Kemner, T. Shibata and B.A. Bunker, *J. Phys. Chem. A*, 108 (2004) 5131. <https://doi.org/10.1021/jp049444y>.
34. R. Jiang, Y. Wang, X. Wen, C. Chen and J. Zhao, *Appl. Surf. Sci.*, 412 (2017) 214. <https://doi.org/10.1016/j.apsusc.2017.03.155>.
35. F. Mohammadi, T. Nickchi, M.M. Attar and A. Alfantazi, *Electrochim. Acta*, 56 (2011) 8727. <https://doi.org/10.1016/j.electacta.2011.07.072>.
36. H.-H. Ge, G.-D. Zhou and W.-Q. Wu, *Appl. Surf. Sci.*, 211 (2003) 321. [https://doi.org/10.1016/S0169-4332\(03\)00355-6](https://doi.org/10.1016/S0169-4332(03)00355-6).
37. A. Fattah-alhosseini, F. Soltani, F. Shirsalimi, B. Ezadi and N. Attarzadeh, *Corrosion Sci.*, 53 (2011) 3186. <https://doi.org/10.1016/j.corsci.2011.05.063>.
38. G.J. Brug, A.L.G. Van Den Eeden, M. Sluyters-Rehbach and J.H. Sluyters, *J. Electroanal. Chem.*, 176 (1984) 275. [https://doi.org/10.1016/S0022-0728\(84\)80324-1](https://doi.org/10.1016/S0022-0728(84)80324-1).
39. M.K. Mishra, G. Gunasekaran, A.G. Rao, B.P. Kashyap and N. Prabhu, *J. Mater. Eng. Perform.*, 26 (2017) 849. <https://doi.org/10.1007/s11665-016-2470-0>.
40. N. Soltani, N. Tavakkoli, M.K. Kashani, A. Mosavizadeh, E.E. Oguzie and M.R. Jalali, *J. Ind. Eng. Chem.*, 20 (2014) 3217. <https://doi.org/10.1016/j.jiec.2013.12.002>.
41. J. Porcayo-Calderon, I. Regla, E. Vazquez-Velez, L.M. Martinez de la Escalera, J. Canto and M. Casales-Diaz, *J. Spectr.*, vol. 2015, Article ID 184140, 13 pages, 2015. <https://doi.org/10.1155/2015/184140>.

© 2020 The Authors. Published by ESG (www.electrochemsci.org). This article is an open access article distributed under the terms and conditions of the Creative Commons Attribution license (<http://creativecommons.org/licenses/by/4.0/>).